

Article

Synthesis of Silver Nanoparticles Using Green Reducing Agent: Ceylon Olive (*Elaeocarpus serratus*): Characterization and Investigating Their Antimicrobial Properties

Kumudu M. Fernando ^{1,*}, Chamila A. Gunathilake ^{2,*}, Chandi Yalegama ¹, Upeka K. Samarakoon ³, Chacrawarthise A. N. Fernando ^{3,4}, Gangani Weerasinghe ¹, Geethi K. Pamunuwa ⁵, Ibrahim Soliman ⁶, Nomi Ghulamullah ², Suranga M. Rajapaksha ⁷ and Omar Fatani ²

¹ Coconut Research Institute, Lunuwila 61150, Sri Lanka; cyalegama@yahoo.com (C.Y.); tmsgweerasinghe@yahoo.com (G.W.)

² College of Aeronautics & Engineering, Kent State University, Kent, OH 44242, USA; nghulamu@kent.edu (N.G.); ofatani@kent.edu (O.F.)

³ Department of Nano Science Technology, Faculty of Technology, Wayamba University of Sri Lanka, Kuliypitiya 60200, Sri Lanka; upeka@wyb.ac.lk (U.K.S.); canfernando9@wyb.ac.lk or fernando.can@kdu.ac.lk (C.A.N.F.)

⁴ Department of Marine Engineering, Faculty of Engineering, General Sir John Kotelawala Defense University, Rathmalana 10390, Sri Lanka

⁵ Department of Horticulture and Landscape Gardening, Faculty of Agriculture and Plantation Management, Wayamba University of Sri Lanka, Makandura 81070, Sri Lanka; geethip@wyb.ac.lk

⁶ Advanced Materials and Liquid Crystal Institute, Kent State University, Kent, OH 44240, USA; isoliman@kent.edu

⁷ Department of Materials and Mechanical Technology, Faculty of Technology, University of Sri Jayewardenepura, Homagama 10200, Sri Lanka; suranga@sjp.ac.lk

* Correspondence: jakmfernando@wyb.ac.lk (K.M.F.); cgunathi@kent.edu (C.A.G.); Tel.: +94-712931927 (K.M.F.); +1-3304229226 (C.A.G.)



Citation: Fernando, K.M.;

Gunathilake, C.A.; Yalegama, C.; Samarakoon, U.K.; Fernando, C.A.N.; Weerasinghe, G.; Pamunuwa, G.K.; Soliman, I.; Ghulamullah, N.; Rajapaksha, S.M.; et al. Synthesis of Silver Nanoparticles Using Green Reducing Agent: Ceylon Olive (*Elaeocarpus serratus*): Characterization and Investigating Their Antimicrobial Properties. *J. Compos. Sci.* **2024**, *8*, 43. <https://doi.org/10.3390/jcs8020043>

Academic Editor: Francesco Tornabene

Received: 16 December 2023

Revised: 14 January 2024

Accepted: 19 January 2024

Published: 24 January 2024



Copyright: © 2024 by the authors. Licensee MDPI, Basel, Switzerland. This article is an open access article distributed under the terms and conditions of the Creative Commons Attribution (CC BY) license (<https://creativecommons.org/licenses/by/4.0/>).

Abstract: Silver nanoparticles (AgNPs) are widely recognized as a prominent antimicrobial agent and have found applications in the field of medicine. This study focuses on the synthesis of AgNPs utilizing the natural reducing agent of Ceylon olive (*Elaeocarpus serratus*), presenting an economically viable and ecologically friendly approach. For the first time, this research demonstrated the synthesis of AgNPs using phytochemicals extracted from Ceylon olive, serving as both natural reducing and stabilizing agents. The synthesized AgNPs were characterized with UV–visible spectroscopy, a particle size analyzer (PSA), X-ray diffraction (XRD), Fourier transform infrared spectroscopy (FTIR), and scanning electron microscopy (SEM) coupled with an energy dispersive X-ray spectrometer (EDX). The UV–visible spectra primarily indicated the formation of the AgNPs by the surface plasmon resonance band around 434 nm. SEM analysis confirmed the presence of silver nanoparticles within a size range of 50–110 nm, with an average size of approximately 70 nm. FTIR determined that proteins, phenols, and flavonoids may have acted as reducing and capping agents. Experimental parameters were optimized to improve the yield and size of the AgNPs and eventually evaluate their antibacterial properties. The well diffusion method exhibits a significantly larger zone of inhibition for Gram-negative bacterial strains (18.4 ± 0.55 mm for *Pseudomonas aeruginosa* and 14.4 ± 0.55 mm for *Escherichia coli*) compared to Gram-positive bacterial strains (11.6 ± 0.55 mm for *Staphylococcus aureus* and 10.4 ± 0.55 mm for *Staphylococcus epidermidis*) for 50 µg/mL AgNPs. These findings demonstrate that AgNPs synthesized with Ceylon olive have the potential to develop into novel materials for bacterial-mediated diseases.

Keywords: antimicrobial activity; Ceylon olive; green synthesis; silver nanoparticles

1. Introduction

In the current scenario, there has been a notable surge in global interest surrounding nanostructured metallic nanoparticles, mainly in the fields of nanomedicine [1] and material science, owing to their exceptionally high surface-area-to-volume ratio [2]. Among the metallic nanoparticles, silver metallic nanoparticles (AgNPs) have gained much interest for biomedical [1] and nanocomposite [3] applications due to their exceptional bactericidal properties [4].

Nanotechnology encompasses a diverse array of methodologies, including chemical, physical (including laser ablation [5], mechanical milling [6], gas-phase beams and magnetron sputtering [7], cluster beam deposition [8], and magnetron sputtering and supersonic cluster beam deposition [9]), as well as biological approaches (green synthesis and microbial synthesis) to facilitate the synthesis of metallic nanoparticles. While conventional chemical methods have long been recognized for their crucial role in nanoparticle production, it is acknowledged that certain chemicals used in these methods can produce toxic by-products, posing significant environmental risks. Furthermore, chemical synthesis techniques may lead to the presence of harmful chemical species adsorbed onto the nanoparticle surfaces. This occurrence limits the therapeutic and clinical applications of these nanoparticles [10]. In parallel, previous studies have indicated that specific physical procedures entail elevated temperatures and substantial energy consumption [11,12].

In the realm of microbial synthesis, the process becomes time-intensive due to the necessary culture preparation and maintenance, distinguishing it from the more efficient green synthesis method utilizing plant extracts [13,14]. Consequently, green synthesis stands out as the preferred choice for nanoparticle fabrication when compared to physicochemical [15] and microbial alternatives. This preference for green synthesis is attributed to its cost-effectiveness, minimal energy requirements, eco-friendliness, and inherent scalability for bulk production, achievable through artificial neural network modeling [16,17]. Given these considerations, the pursuit of research into the green synthesis of silver nanoparticles (AgNPs) using plant extracts is paramount to fulfill the growing demand for these materials. Previous literature has reported the utilization of various fruit extracts in the synthesis of silver nanoparticles. These extracts include *Aegle marmelos* [18], *Cordia obliqua* Willd [19], *Glycosmis pentaphylla* [20], *Phyllanthus emblica* [21], *Diospyros malabarica* [22], *Garcinia mangostana* [23], and *Manilkara zapota* [24]. Similarly, leaf extracts from plants such as *Cannabis sativa* [25], *Cucumis prophetarum* [26], *Origanum majorana* [27], *Acer oblongifolium* plant extract [28], *Hagenia abyssinica* [29], and *Muntingia calabura* [30] have also been explored for this purpose. Additionally, Fernando et al. [31] conducted a study on the nutritional composition, bioactive compounds, and antimicrobial effects of *Elaeocarpus serratus* fruit extract. Biswas et al. [32] investigated the phytochemicals and determined the cytotoxicity and antimicrobial effects of the ethanol extract of *Elaeocarpus serratus*. Their findings revealed that *Elaeocarpus serratus* primarily consists of alkaloids, glycosides, tannins, saponins, flavonoids, and carbohydrates. The ethanol extract of *Elaeocarpus serratus* exhibited potential antibacterial and cytotoxic properties. Moreover, Jayashree et al. [33] explored the presence of bioactive compounds in acetone, methanol, and water extracts of the leaf, stem bark, and fruit of *Elaeocarpus serratus* L. They also studied the antimicrobial activity of these extracts. Manoharan et al. [34] investigated the antioxidant and antimicrobial effects of *Elaeocarpus tectorius* (Lour.) fruit extract against urinary tract infection pathogens. Geetha et al. [35] identified phytochemicals in the leaves of *Elaeocarpus serratus*. Sircar et al. [36] focused on the antibacterial activity of silver nanoparticles synthesized from the fruit, seed, and mesocarp–epicarp extract of *Elaeocarpus floribundus*, a species of the Elaeocarpaceae family. Their study suggested that these synthesized nanoparticles have the potential to combat bacterial drug resistance and infections. Furthermore, Kumar et al. [37] evaluated the antioxidant properties of *Elaeocarpus ganitrus* Roxb. leaves, finding significant antioxidant activity attributed to phenolics and flavonoids. *Elaeocarpus ganitrus* Roxb. was also investigated for pharmacognostic and antifungal activity [38]. However, it is noteworthy that, to date, there has been no investigation into the synthesis of silver

nanoparticles (AgNPs) using the fruit extract from the species of *Elaeocarpus serratus* (Ceylon olive). Therefore, in this study, we utilize the extract from Ceylon olive fruits as a green reducing agent to synthesize AgNPs.

Ceylon olive (*Elaeocarpus serratus*) is a highly abundant indigenous plant of Sri Lanka. The fruit of Ceylon olive exhibits medicinal and antioxidant properties as it has a tremendous amount of valuable constituents such as flavonoids, condensed tannins, carotenoids, vitamin C, minerals, and anthocyanins, of which some are beneficial for the prevention of cancer, cardiovascular diseases, diabetes, neurodegenerative diseases (such as Alzheimer's disease), osteoporosis, aging, and cataracts [39]. Despite the fact that many researchers looked into the medicinal and healing benefits of the plant and the nutritive value of the fruit, no exploration was made of its oxidative property. Modifying the chemical state, like the ionization of the reduction process in the synthesis of AgNPs, highly affects the effectiveness of the formation of AgNPs. In this regard, optimizing the synthesis processes of AgNPs, including the concentration of plant extract, pH, and temperature of the medium, is crucial for achieving a good yield. This involves producing a significant quantity of nanoparticles with regulated size and stability, ensuring consistency in size throughout the synthesis process. Therefore, the primary objective of this study was to assess the viability of employing Ceylon olive fruit extract in the synthesis of AgNPs under optimal processing parameters. Additionally, the synthesized AgNPs were subjected to comprehensive characterization using techniques such as UV-visible spectroscopy, particle size analysis (PSA), X-ray diffraction (XRD), and Fourier transform infrared spectroscopy (FTIR). Furthermore, an analysis was conducted to evaluate the antimicrobial efficacy of the synthesized AgNPs against human pathogenic bacteria.

2. Materials and Methods

2.1. Materials

Silver nitrate ($\text{AgNO}_3 \geq 99\%$) and hydrochloric acid ($\text{HCl} \geq 37\%$) were purchased from Sigma Aldrich, USA and analytical-grade sodium hydroxide (NaOH) was purchased from Fisher Scientific (Pvt) Ltd, UK. Mature Ceylon olive fruits were collected from Wayamba University of Sri Lanka, Kuliapitiya. The bacterial cultures of *Escherichia coli* and *Pseudomonas aeruginosa* were obtained from the University of Kelaniya, Sri Lanka, while *Staphylococcus epidermidis* and *Staphylococcus aureus* were obtained from Wayamba University of Sri Lanka, Makandura. Ultra-pure water (Milli-Q water) was used for all the experiments.

2.2. Preparation of Ceylon Olive Fruit Extract

Mature Ceylon olives were washed well using Milli-Q water, and seeds were removed from the olive fruits. The flesh of the Ceylon olive fruits was crushed using a grinder and then blended by mixing with Milli-Q water (1:5; flesh:Milli-Q water). The contents were heated in a shaking water bath at $80\text{ }^\circ\text{C}$ for 30 min. Subsequently, the mixture was subjected to centrifugation at 4000 rpm for 20 min using a Centurion PRO-HOSP.LLR centrifuge (UK) to eliminate any residual matter. The supernatant was filtered through Whatman No. 1 filter papers to obtain a clear solution, which was subsequently stored at $4\text{ }^\circ\text{C}$. This prepared solution was used for the reduction of silver ions in AgNO_3 .

2.3. Synthesis of AgNPs with Optimization of Process Parameters

The synthesis of AgNPs was conducted using the following protocol:

2.3.1. Effect of the Volume of Ceylon Olive Fruit Extract on the Formation of Silver Nanoparticles

For the synthesis of AgNPs, we followed the procedure outlined by Calhan and Gundogan, with necessary adjustments [40]. For this study, $5\text{ }\mu\text{L}$ of the fruit extract per drop was introduced to accommodate the inclusion of the sample volume. A conical flask with a solution of 40 mL of 1 mM AgNO_3 was heated to $80\text{ }^\circ\text{C}$ using a magnetic stirrer. Ceylon olive fruit extract ($110\text{ }\mu\text{L}$) was added dropwise to the AgNO_3 solution at $80\text{ }^\circ\text{C}$ using

a micropipette while stirring vigorously. After the addition was completed, the contents were further stirred for about 20 min. The formation of AgNPs was confirmed by the color change in AgNO₃ from colorless to yellowish brown. The experiment was repeated with 130, 150, and 170 µL of fruit extract. The absorbance spectra of the synthesized AgNP samples were obtained in the wavelength range of 300–800 nm using a UV–Vis spectrophotometer (Shimadzu, UV 1800, Japan). Milli-Q water was used as the reference.

2.3.2. Effect of Temperature on the Formation of AgNPs

Elevated temperatures accelerate chemical reactions, influencing the rate of nucleation and growth of nanoparticles. To investigate this effect, we synthesized AgNPs at different temperatures. For the optimization of temperature, a solution of 40 mL of 1 mM AgNO₃ was heated to 40 °C. The pH of the AgNO₃ solution was adjusted to 6. Subsequently, 150 µL of the fruit extract (the optimal volume determined in Section 2.3.1) was added dropwise (5 µL of fruit extract per drop) to the AgNO₃ solution at 40 °C using a micropipette. Vigorous stirring was maintained throughout this process. After adding fruit extract, the solution was continuously stirred for an additional 20 min to induce a color change in the AgNO₃ solution from colorless to yellowish brown. The experiment was conducted at different temperatures: 50 °C, 60 °C, and 70 °C for the AgNO₃ solution. The optimum temperature was confirmed through UV–Vis spectrophotometer analysis.

2.3.3. Effect of pH on the Formation of AgNPs

To find the effect of pH, the following procedure was employed: A 0.1 N NaOH solution was added to adjust the pH of a 40 mL of 1 mM AgNO₃ solution to 5 and the solution was subsequently heated to 60 °C (the optimal temperature determined in Section 2.3.2). Using a micropipette, 150 µL (the ideal volume determined from Section 2.3.1) of the fruit extract was added dropwise to the AgNO₃ solution while vigorously swirling at 60 °C. After that, the mixture was agitated for an additional 20 min to turn AgNO₃ from colorless to yellowish brown. The experiment was repeated at different pH values of 6, 7, and 8. The optimum pH value was confirmed by UV–Vis spectrophotometer analysis.

2.4. Characterization of AgNPs

The generated AgNPs were centrifuged at 14,000 rpm for 15 min in order to separate the supernatant and characterize the AgNPs. To get rid of organic matter attached to AgNPs, centrifugation was used to wash the solid particles with acetone and Milli-Q water. Upon removing the supernatants, the solid particles were separated. In the preparation for future use, AgNPs were dried and kept at room temperature in a dark environment.

The particle size and morphology of the AgNPs were characterized using a laser diffraction particle size analyzer (PSA), X-ray diffraction (XRD), Fourier transform infrared spectroscopy (FTIR), and a scanning electron microscope (SEM) coupled with energy dispersive X-ray spectroscopy (EDX).

2.4.1. Particle Size Analysis

Particle size analysis was performed by a laser diffraction particle size analyzer (Fritsch Analysette 22 nano Plus, Germany) in the wet method. The samples were irradiated with incident light, and the detectors recorded the energy scattered and absorbed at particular angles.

2.4.2. X-ray Diffraction (XRD) Structural Analysis

The crystalline property of synthesized AgNPs was identified by X-ray diffraction measurement. AgNPs were first added to a quartz sample holder, and analysis was performed using Cu-K α radiation at 40 kV and 30 mA. The data were taken at a 2 θ range of 20–80 °C. The mean particle size was calculated using the derivation of the Williamson–Hall uniform deformation model (WH-UDM) as given in Equation (1) [41].

$$\beta \cos \theta = 4\epsilon \sin \theta + (K\lambda)/D \quad (1)$$

where D , K , ε , and λ denote crystallite size, shape factor ($K = 0.9$), lattice strain, and X-ray wavelength ($\lambda = 1.5406$ nm), respectively. The crystalline structure was determined by considering the intercept of the plot ($K\lambda/D$) [41].

2.4.3. Scanning Electron Microscopy Equipped with Energy Dispersive Spectroscopic (SEM-EDX) Analysis

The surface morphology of AgNPs was examined using a scanning electron microscope (Carl Zeiss EVO 18 Research). To prepare the sample, dried silver nanoparticle material was placed onto a conductive carbon tape, which was fixed to an aluminum sample stub. Subsequently, the sample was covered with a gold–palladium coating. The composition of AgNPs was examined using an EDX (Carl Zeiss Evo 18 Research) system equipped with a SEM.

2.4.4. Fourier Transform Infrared (FTIR) Analysis

FTIR determined the functional groups of the samples. It can be used to identify the reduction of silver ions. FTIR spectra of powdered AgNPs were obtained using a Shimadzu IR Affinity -1S spectrophotometer. The samples were mixed with KBr to form pellets, and the spectra were recorded at a wavenumber ranging from 4000 to 400 cm^{-1} .

2.5. Antimicrobial Activity

The antimicrobial activity of silver nanoparticles (AgNPs) was assessed utilizing the agar-well diffusion method, as outlined in the study conducted by Rautela et al. [42], with certain modifications. The study employed Gram-negative bacterial strains, namely *Escherichia coli* (*E. coli*) and *Pseudomonas aeruginosa* (*P. aeruginosa*), as well as Gram-positive bacterial strains, including *Staphylococcus aureus* (*S. aureus*) and *Staphylococcus epidermidis* (*S. epidermidis*). To carry out the procedure, a sterile spreader was employed to evenly distribute 100 μL of each bacterial strain, containing a concentration of 2.6×10^7 colony-forming units per milliliter (CFU/mL), onto nutrient agar plates. For the purpose of analysis, four wells, each with a diameter of 5 mm, were created in the agar plate using a cork borer. Subsequently, each well was filled with 80 μL of the following samples, having a concentration of 50 $\mu\text{g}/\text{mL}$: AgNPs, Ceylon olive extract, AgNO_3 , and streptomycin which served as the control. The evaluation of the antimicrobial effect was based on the appearance of a clear zone, referred to as an inhibition zone, around each well. This zone indicated the extent of inhibition caused by the respective samples against the growth of the bacterial strains under investigation. The experiment was carried out in five replicates.

Minimum Inhibitory Concentration (MIC)

The term MIC refers to the lowest amount of a substance needed to prevent microbes from growing visibly after an overnight incubation. This study was conducted using the methodology described by Rautela et al. for the determination of MIC [42].

Six sterilized test tubes containing 5 mL of nutrient broth medium were added with varying concentrations of AgNPs, such as 30, 15, 7.5, 3.75, and 1.875 $\mu\text{g}/\text{mL}$ and one test tube was kept as a control. They were inoculated with an equal volume (200 μL) of microbial culture samples with an optical density of 0.5. These samples were incubated in a shaker incubator at 250 rpm and maintained at 37 $^\circ\text{C}$ for 24 h. This procedure was performed in triplicate for all four samples of both Gram-negative and Gram-positive bacteria. Absorbance measurements were taken at a wavelength of 600 nm, and the data were utilized to create a graph plotting optical density against the concentration of AgNPs. The point at which the optical density reached its lowest value indicated the MIC of AgNPs.

To corroborate the results, a further validation step involved the examination of visible colonies using the agar plate method [43]. This verification was conducted for the bacterial culture test tubes that exhibited the lowest optical densities, ensuring the absence of bacterial growth.

2.6. Statistical Analysis

The diameters of inhibition zones in the antimicrobial activity assessment were given as mean \pm SD (SD: standard deviation). One-way ANOVA was carried out using the MINITAB 17 version of Tukey's pairwise comparison test at a $p < 0.05$ confidence level.

3. Results and Discussion

3.1. Characterization of AgNPs

3.1.1. SEM-EDX Analysis

Scanning electron microscopy (SEM) analysis is an effective technique for investigating material surface morphology. In this study, SEM analysis was employed to examine the surface morphology of AgNPs and the structural characteristics of the Ag particles, illustrated in Figure 1, reveal that the sizes of these nanoparticles fall within the range of 50–110 nm, with an average size of approximately 70 nm, exhibiting a diverse range of shapes. Notably, AgNPs exhibited an irregular shape and demonstrated excellent dispersion, attributed to the coating of nanoparticles by biomolecules. Some AgNPs were found to exhibit cubic and pebble-like forms [44], depending on parameters such as pH, temperature, and extract concentration. However, small clusters of particles were observable due to the tendency of nanoparticles to agglomerate owing to their heightened surface energy, aiming to minimize surface energy [45]. Comparable outcomes were documented in the investigation of AgNP synthesis employing *Annona squamosa* leaf extract [46]. Additionally, Vander Waals forces might have been aroused between the phytochemicals employed for reducing metallic particles, as detailed in reference [47].

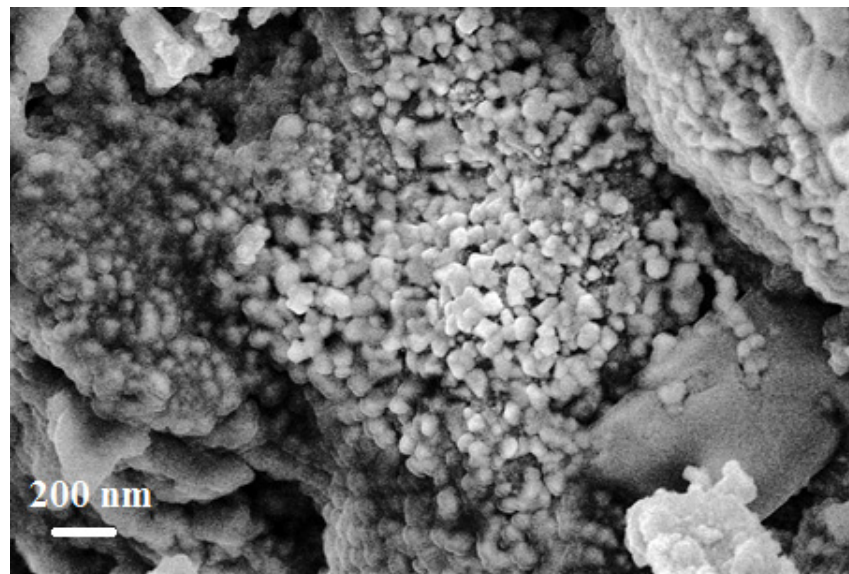


Figure 1. SEM image of AgNPs synthesized using Ceylon olive extract and 1 mM AgNO₃.

The EDX graph is a vital tool in the green synthesis of AgNPs, as it provides crucial information about the elemental composition and purity of the nanoparticles generated. EDX measurement (Figure 2) revealed the characteristic energy absorption peaks of AgNPs at roughly 3 keV due to surface plasmon resonance. The study conducted by Femi-Adepoju et al. has confirmed our finding by determining the optical absorption peak for AgNPs at roughly 3 keV [48]. A high absorption peak for metallic silver ions in the 2.5–3.7 keV range was reported by Sarwer et al. in their study [49].

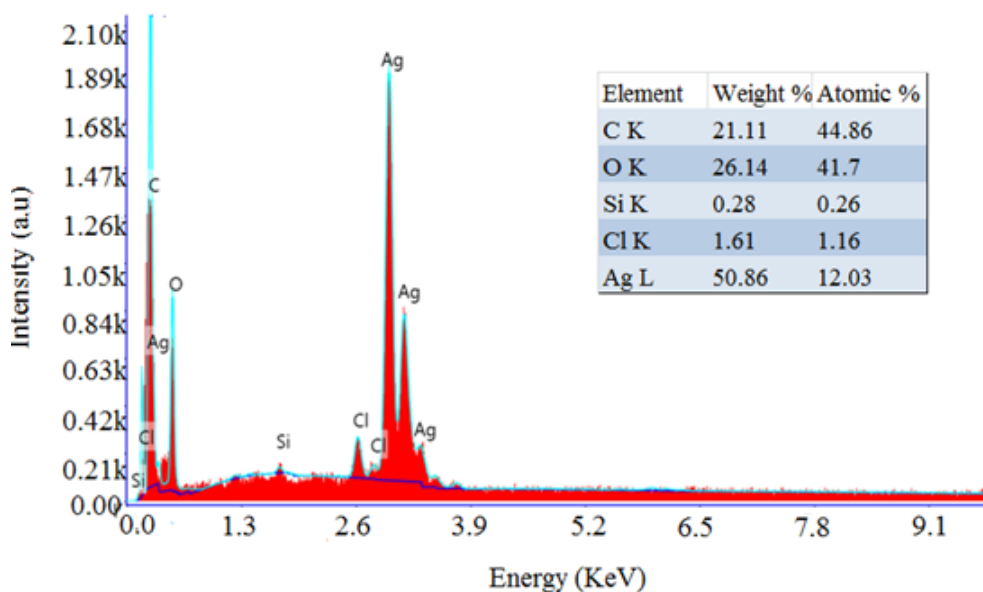


Figure 2. Energy dispersive X-ray spectroscopy of the AgNPs.

3.1.2. XRD Analysis

The crystallinity of green synthesized AgNPs was ascertained by an XRD study (Figure 3). Bragg's reflection peaks at 38.26° , 46.23° , 64.47° , 77.54° , and 81.71° were indexed with respect to five intense peaks of (111), (200), (220), (311), and (222). These peaks were well matched with the study reported by Ravichandran et al. on the synthesis of AgNPs [50]. The peaks corresponded to the face-centered cubic (FCC) structure of AgNPs with reference to Joint Committee on Powder Diffraction Standards (JCPDS) file no. 04-0783. These five intense peaks observed for the synthesized AgNPs were comparable to those in the study conducted by Mohammed et al. in the synthesis of AgNPs with *Lycium shawii* leaf extract [51]. The average particle size of Ag crystallite was found to be 19 nm using the graphical method given in Section 2.4.2. A similar result (average size of 19 nm) was reported in the synthesis of AgNPs using *Piper chaba* stem extracts [52]. Actually, the crystallite size was highly dependent on the XRD peak values, which were indirectly caused by the reducing and capping agents of phytochemicals in the extracts used for the synthesized AgNPs.

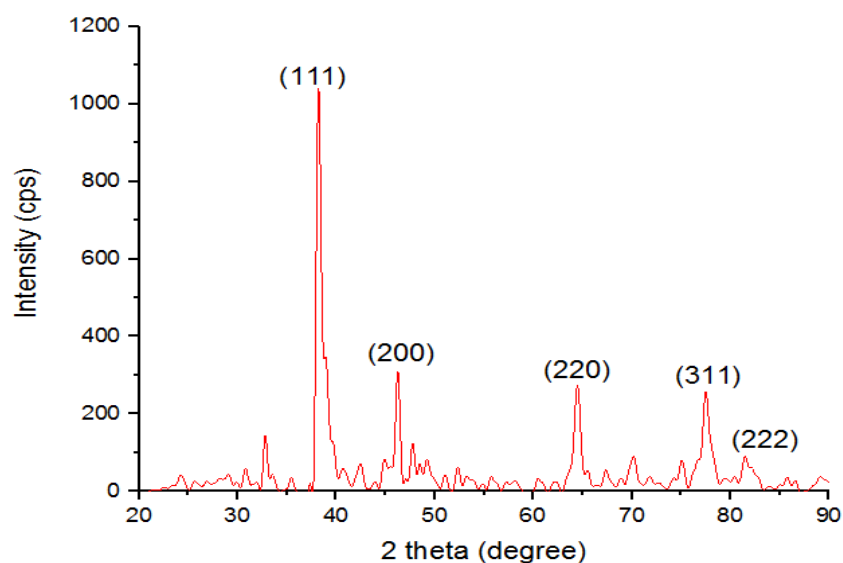


Figure 3. XRD spectrum of synthesized AgNPs using Ceylon olive extract.

3.1.3. FTIR Analysis

FTIR is a universal technique for the identification of functional groups in organic or inorganic materials. It determines the distinct absorption and transmission peaks relevant to the frequencies of vibration between the bonds of the particles of a material. FTIR analysis was performed to investigate the functional groups of Ceylon olive extract responsible for reducing and stabilizing AgNPs. Figure 4 (a, b) show the FTIR spectra of Ceylon olive fruit extract and synthesized AgNPs. As shown in Figure 4 (a), strong absorption peaks appeared at 1041, 1250, 1625, 1729, and 3431 cm^{-1} . The peaks observed in the extract shifted toward the higher wavenumber side, such as 1049, 1259, 1651, 1797, and 3475 cm^{-1} , respectively. The binding of phytochemicals to the AgNPs can be proved not only due to the shifting of peaks to higher wavelengths such as 1041 to 1049 cm^{-1} , 1250 to 1259 cm^{-1} , 1625 to 1651 cm^{-1} , 1729 to 1797 cm^{-1} , and 3431 to 3475 cm^{-1} but also due to the reduction of peak height [53]. The peak value at 1049 cm^{-1} was assigned to the C-O stretch of the alcoholic group. The peak at 1250 cm^{-1} corresponded to the vibration of the C-O group of the hydroxyl flavonoids [54] and was shifted to 1259 cm^{-1} , inferring the involvement of flavonoids in the synthesis of AgNPs. The -OH group of flavonoids has the ability to release electrons when inducing light energy, leading to reducing silver ions (Ag^+) to silver elementary materials (Ag^0) [55]. The peak at 1651 cm^{-1} was characteristic of the N-H bending vibration found in polypeptides of protein [56]. The peak at 3475 cm^{-1} can be attributed to the stretching vibrations of alcohols and phenolic compounds [57]. The peak at 1473 cm^{-1} was due to stretching vibrations of aliphatic amines [58]. These observations confirmed that functional groups of carboxyl (-C=O) and amine (N-H) found in amide linkages of proteins, flavonoids, and phenols were successfully bound to AgNPs and stabilized their structure by preventing aggregation. Interestingly, the presence of these protein, flavonoid, and phenol compounds was found in Ceylon olive fruit extract, verified through GC-MS analysis in the study conducted by Fernando et al. [31]. Similar results regarding the binding of these compounds to AgNPs were obtained in a previous study that focused on the synthesis of AgNPs using *Nicotiana tabacum* leaf extract [59].

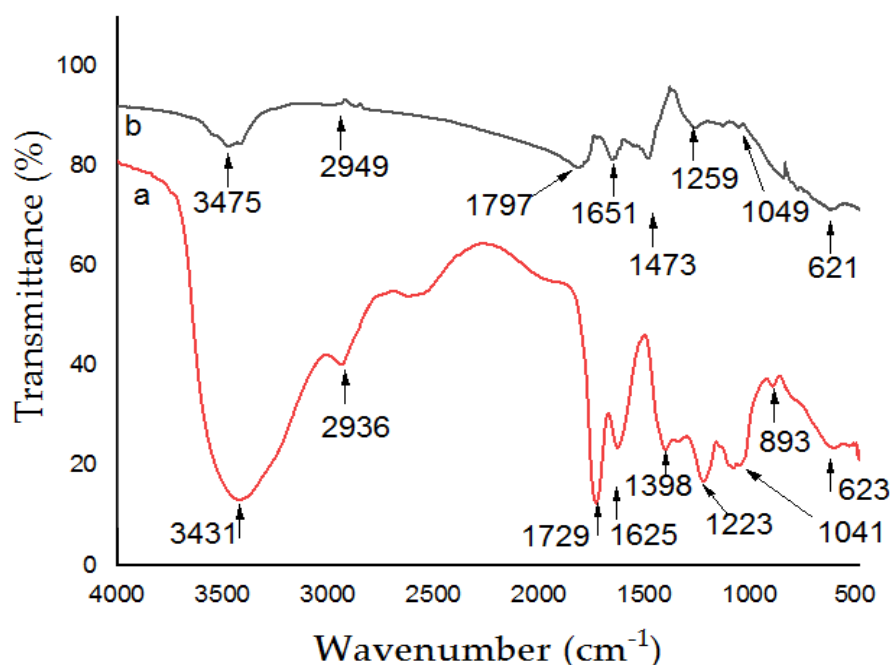


Figure 4. FTIR spectra of (a) Ceylon olive extract and (b) synthesized AgNPs.

3.1.4. Particle Size Analysis

The findings of the wet dispersion laser particle size study of AgNPs are presented in Figure 5. The Gaussian distribution depicted in Figure 5 indicates that the average nanopar-

ticle (NP) size falls within the range of 20 to 25 nm. Upon statistical analysis, it was revealed that the average NP size, conforming to a Gaussian distribution, is approximately 23 nm. These findings imply the promising applicability of the synthesized silver nanoparticles (AgNPs) in diverse fields. However, it is noteworthy that these results deviate from the particle sizes obtained through scanning electron microscopy (SEM). This disparity can be attributed to the agglomeration of silver nanoparticles during the preparation process for SEM analysis, particularly through the drying procedure. The agglomeration phenomenon may lead to an overestimation of particle sizes in SEM images.

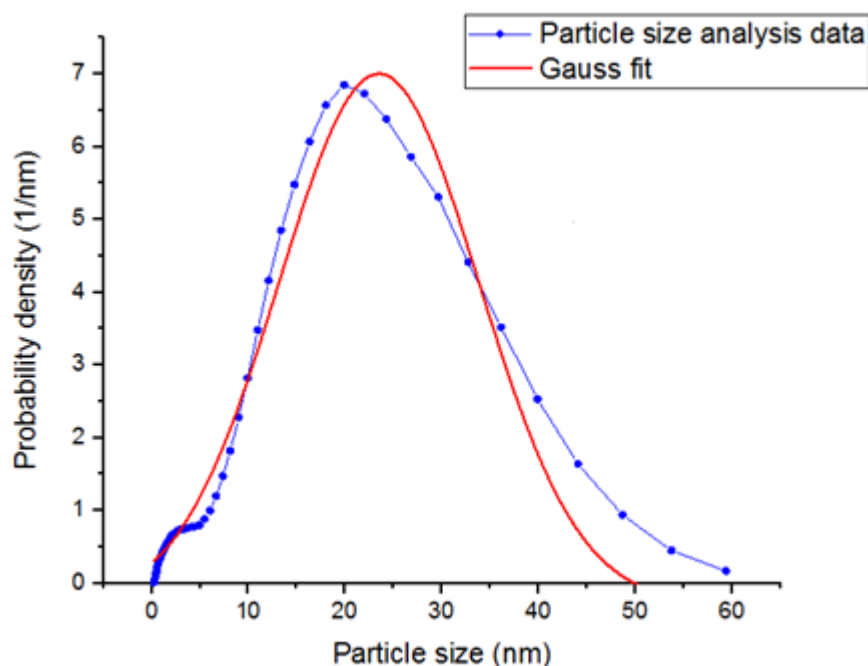


Figure 5. Particle size distribution of silver nanoparticles obtained under optimized condition

3.2. Visual Observation of the Formation of AgNPs

Ceylon olive fruit extract has shown promise as an effective reducing agent for the conversion of AgNO_3 into AgNPs. The gradual addition of the extract to AgNO_3 resulted in a noticeable change in the solution's color, shifting from colorless to yellowish brown within approximately 30 min. This change in color is attributed to the excitation of surface plasmon resonance (SPR) in the silver nanomaterial, providing clear evidence for the formation of AgNPs through the reduction of Ag^+ to Ag^0 [60]. The reduction of Ag^+ to Ag^0 was facilitated by the presence of functional groups such as hydroxyl, carbonyl, and amide groups in various phytochemicals, including enzymes, amino acids, ascorbic acids, proteins, flavonoids, tannins, polyphenols, and carbohydrates found in the fruit extract [61,62]. This reduction process initiated the formation of Ag nuclei, subsequently leading to the synthesis of AgNPs [63].

3.3. Investigation of the Formation of AgNPs with a UV Spectrophotometer

3.3.1. Effect of Volume of Extract on the Formation of AgNPs

Figure 6 shows the UV–visible spectra of AgNPs synthesized using varying volumes of Ceylon olive extract (110, 130, 150, and 170 μL). As the volume of added Ceylon olive extract increased from 110 to 150 μL , the absorbance also increased. This may be due to the higher reduction rate of Ag^+ to Ag^0 to form AgNPs. When increasing the volume of the extract, more functional groups from molecules such as ascorbic acid, flavonoids, tannins, and alkaloids become available as reducing agents for reduction reactions. A single and sharp surface plasmon resonance (SPR) band observed around 434 nm without any shift in the spectrum (Figure 6) confirmed the formation of AgNPs. A single and sharp SPR

band is attributed to the uniform size distribution of stable, isotropic-shaped AgNPs mixed with the capping agents from the Ceylon olive extract. Similar SPR bands were reported in the synthesis of AgNPs using banana peel extract [64] as a reducing agent. Moreover, as the extract volume was increased beyond 150 μL to 170 μL , there was a notable shift in the peak value from 434 to 426 nm, accompanied by a decrease in absorbance. This shift is likely a result of the collective energy absorption effect of organic compounds and nanoparticles in the solution due to the excessive presence of fruit extract. Consequently, this observation highlights the importance of optimizing the amount of extract for the efficient reduction of Ag^+ [65]. It was also noted that the control sample, either silver nitrate or Ceylon olive extract alone, did not exhibit any characteristic SPR band under the given conditions, confirming the absence of AgNPs.

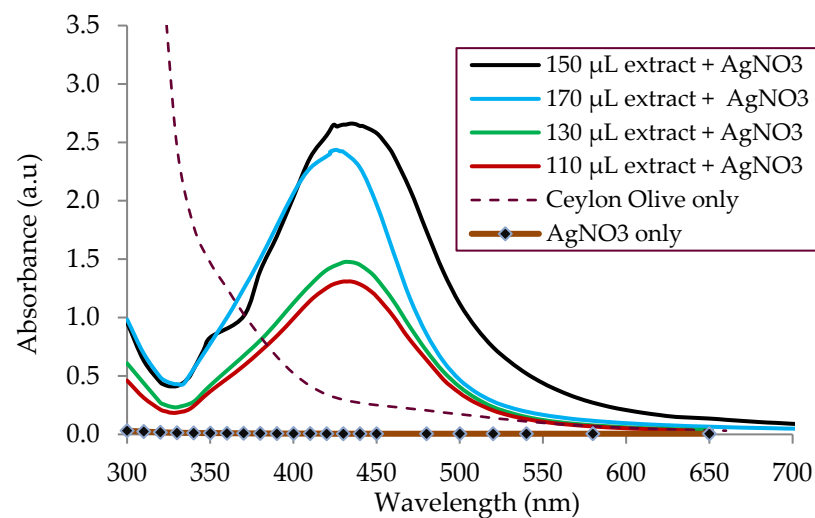


Figure 6. UV-Vis absorption spectra of optimizing volumes of Ceylon olive extract for the synthesis of AgNPs.

3.3.2. Effect of Temperature

Figure 7 illustrates a rise in absorbance with increasing synthesis temperature, ranging from 40 $^{\circ}\text{C}$ to 70 $^{\circ}\text{C}$. This increase can be attributed to the higher formation of nuclei at elevated temperatures, leading to a higher production rate of AgNPs.

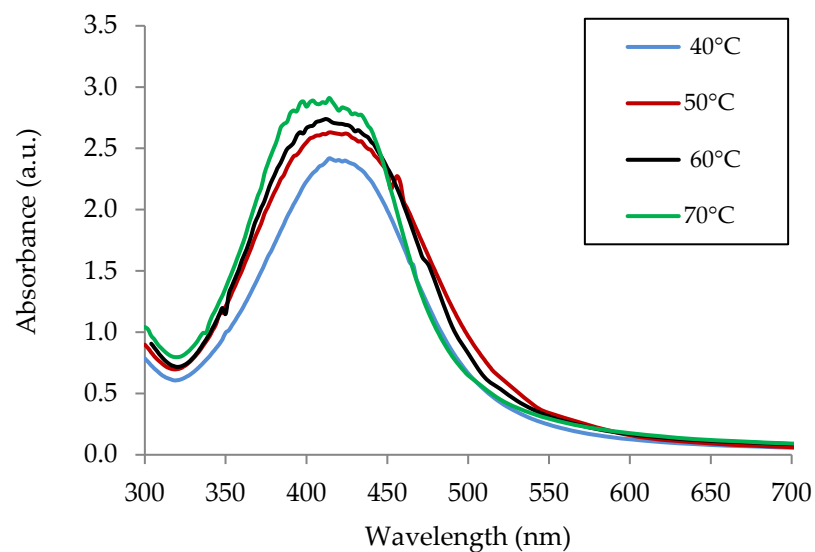


Figure 7. UV-Vis absorption spectra of optimizing temperature for the synthesis of AgNPs.

The absence of peak sharpness in the absorption spectra at 70 °C may be due to the growth of polydisperse nanoparticles. These findings align with previous research on silver nanoparticle synthesis using *Megaphrynium macrostachyum* leaf extract [66]. Therefore, 60 °C was chosen as the ideal temperature to synthesize silver nanoparticles using Ceylon olive extract. This outcome is in line with the outcomes of the synthesis of AgNPs utilizing stem extracts from *Piper chaba* [52].

3.3.3. Effect of pH of Medium for the Formation of the AgNPs

The pH of the medium utilized in nanoparticle synthesis is a critical factor governing the control of nanoparticle size and shape [67]. In this study, the synthesis of AgNPs was investigated at various pH levels to determine the optimal pH value. Figure 8 illustrates the influence of pH on AgNPs' absorbance. As depicted in Figure 8, the spectral peak of surface plasmon resonance (SPR) bands exhibited pH dependence. At pH 5, the absorbance peak was indiscernible, which may be due to the deactivation of biomolecules (e.g., reducing agents) engaged in AgNP synthesis under moderately acidic conditions [65,67]. However, by increasing the pH from 6 to 7, the absorption of AgNPs increased, and the SPR band shifted to a lower wavelength from 412 nm to 410 nm due to the shrinking size of AgNPs [68,69]. Increasing the pH of the synthesis medium affects the nature (electrical charges) of biomolecules and thus the degree of capping and stabilizing, which leads to the formation of more nanoparticles [69]. A further increase in pH to 8 resulted in the formation of an absorption spectrum with a distorted peak, as shown in Figure 8. It might be due to the overlapping of peaks, which is attributed to the polydispersed nanoparticles [66]. Therefore, pH 7 was selected as the optimum pH of the medium for further studies. Our results were in line with the report on the extraction of AgNPs using *Piper chaba* stem extracts [52], which showed that neutral and basic conditions were very appropriate for the reduction reaction, facilitating the synthesis of AgNPs, and further confirmed in a research review written by Vanlalveni et al. [70]. The color variation of the solutions occurred when changing the pH. It can be attributed to the variation in shape and size of AgNPs [71]. The study conducted by Mothana et al. [72] showed that the color of the solution became dark brown at higher pH conditions, mainly at alkaline pH. It is due to the ionization of functional groups available in the extract at high pH. A similar color change was observed in the study conducted by Davidovic et al. concerning silver colloids coated with the polysaccharide dextran [73].

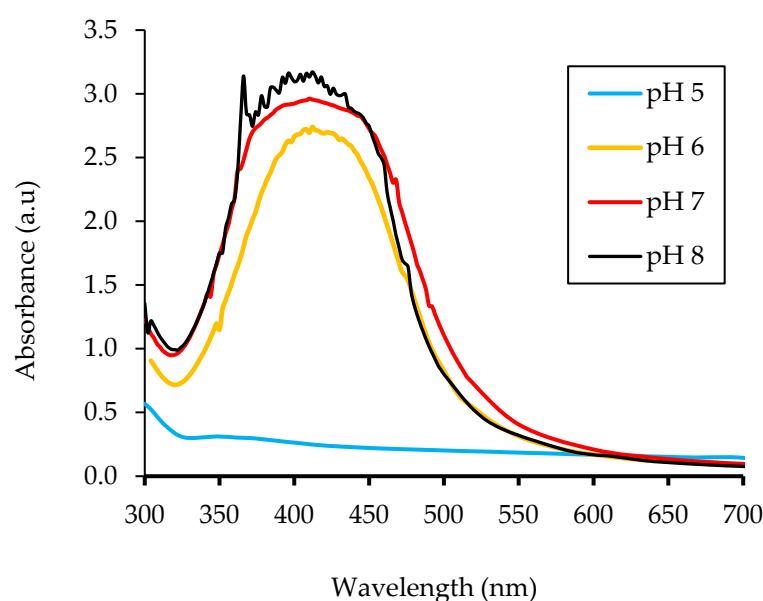


Figure 8. UV-Vis absorption spectra of optimizing pH for the synthesis of AgNPs.

3.4. Antibacterial Activity

Figure 9 and Table 1 display the inhibition zones produced by AgNPs, AgNO₃, Ceylon olive extract, and the control (streptomycin) against the four bacteria. Analysis revealed that AgNPs exhibited significantly larger inhibition zones for Gram-negative bacteria (18.4 ± 0.55 mm for *P. aeruginosa* and 14.4 ± 0.55 mm for *E. coli*) compared to Gram-positive bacteria (11.6 ± 0.55 mm for *S. aureus* and 10.4 ± 0.55 mm for *S. epidermidis*).

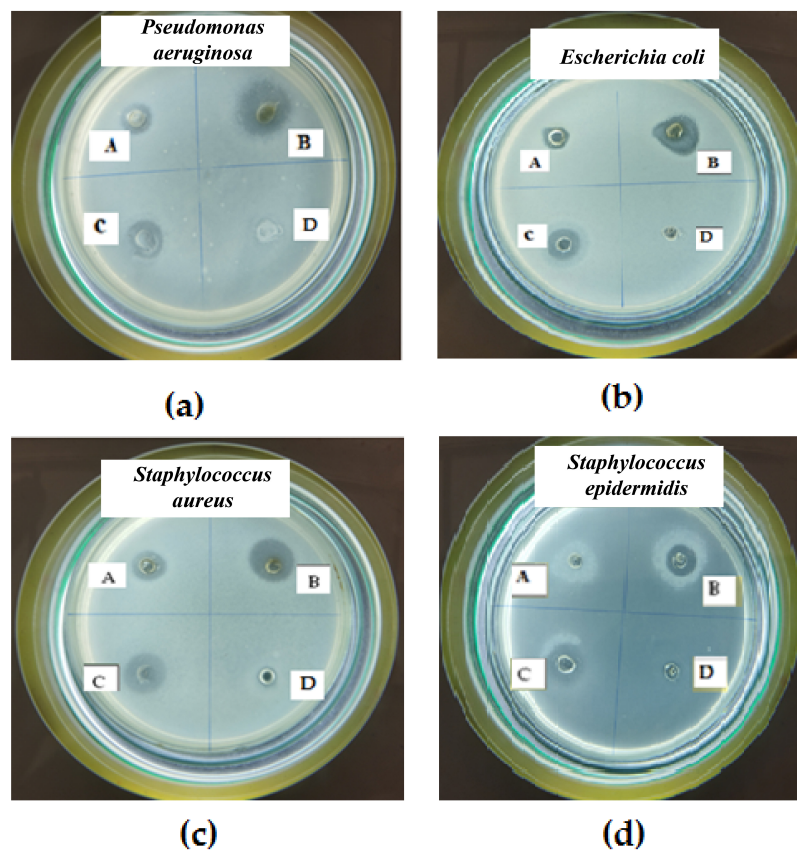


Figure 9. Appearance of zones of inhibition of (A) AgNO₃, (B) AgNPs, (C) control, and (D) Ceylon olive extract against (a) *P. aeruginosa*, (b) *E. coli*, (c) *S. aureus*, and (d) *S. epidermidis*.

Table 1. Diameters of zones of inhibition against selected pathogens.

Sample	Average Diameter of Zones of Inhibition (mm)			
	<i>Pseudomonas aeruginosa</i>	<i>Escherichia coli</i>	<i>Staphylococcus epidermidis</i>	<i>Staphylococcus aureus</i>
AgNPs	18.4 ± 0.55^a	14.4 ± 0.55^a	10.4 ± 0.55^a	11.6 ± 0.55^a
AgNO ₃	13 ± 0.71^b	11.2 ± 0.83^b	7.4 ± 0.49^b	8.4 ± 0.55^b
Streptomycin (control)	14.8 ± 1.92^b	13.8 ± 1.09^b	12.8 ± 0.84^c	10.4 ± 1.14^{ab}
Ceylon olive extract	N.D	N.D	N.D	N.D

Means with different superscripts within the same column are significantly different from each other at the $p < 0.05$ level. (N.D—not detected).

The susceptibility of bacteria to silver nanoparticles (AgNPs) depends on the structural characteristics of their cell walls. In the case of Gram-positive bacteria, the cell wall is constituted by a strong peptidoglycan layer with a linear polysaccharide structure cross-linked with peptides. This arrangement imparts a rigid structure enveloping the cell membrane, establishing a tough barrier that hampers the penetration of AgNPs [12]. Consequently, the inhibition zone observed is comparatively lower. Conversely, Gram-negative bacteria exhibit a thinner peptidoglycan layer, facilitating a more effective penetration of AgNPs and

inhibition of the bacterial growth. This increased permeability leads to a correspondingly larger inhibition zone as compared to Gram-positive bacteria. This finding aligns with a study conducted by More et al. [74]. The surface charge of AgNPs might also have a bactericidal effect [75]. AgNPs exhibited a significantly larger zone of inhibition compared to AgNO₃, while streptomycin exhibits no significant difference compared to AgNO₃ against *P. aeruginosa*, *E. coli*, and *S. aureus*. The increased inhibition zones observed for AgNPs may be attributed to the enhanced diffusion capability of small AgNPs within the bacterial agar medium. These nanoparticles can penetrate bacterial cells and interact with DNA, thiol groups, and proteins, leading to enzyme inactivation and bacterial cell death by disrupting cellular metabolism [50,76]. Similar outcomes were observed with AgNPs synthesized using *Cleome viscosa* plant extract [77]. Notably, the Ceylon olive extract did not exhibit antimicrobial effects, possibly due to its low concentration in aqueous form, which may contain fewer phytochemicals compared to ethanolic or methanolic extracts.

The broth dilution technique is used to determine the MIC of AgNPs against bacterial strains. By considering both the lowest optical density values and the visual observation of the absence of bacterial colony growth using the agar plate method, the MIC was found to be 7.5 µg/mL for *E. coli* and *P. aeruginosa* with optical densities of 0.015 ± 0.003 and 0.004 ± 0.001 , respectively. In contrast, for *S. aureus* and *S. epidermidis*, the MIC was found to be 15 µg/mL, accompanied by optical densities of 0.05 ± 0.004 and 0.06 ± 0.01 , respectively (Figure 10). Notably, AgNPs exhibited a more potent inhibitory effect on Gram-negative bacteria compared to Gram-positive bacteria. These findings align with the results of a study conducted by Gopinath et al., which focused on the biosynthesis of AgNPs using the bacterial isolate *Exiguobacterium* sp. KNU1 [78,79]. In their study, they found that AgNPs inhibited the growth of Gram-negative bacteria (*E. coli* at 6.25 µg/mL and *P. aeruginosa* at 7.5 µg/mL) more effectively than Gram-positive bacteria (*S. aureus* at 9 µg/mL). These results agree with our findings. Moreover, a larger clear zone was linked to a lower MIC value, indicating a strong connection between these two parameters. Rautela et al. [42] conducted a study on the minimum inhibitory concentration (MIC) of AgNPs for *E. coli* and *S. aureus*, reporting values of 2.0 µg/mL and 2.6 µg/mL, respectively. In our study, we obtained MIC values that were notably higher than those reported by Rautela et al. The observed variation in MIC values may be attributed to several factors, including differences in experimental conditions, methodologies of the synthesized nanoparticles, and potentially the specific bacterial strains employed in our study compared to those in [42]. Recognizing the influence of strain variations in bacterial species and the variation in the shape of the synthesized AgNPs, it is reasonable to conclude that such distinctions can contribute to variations in susceptibility to antimicrobial agents [62].

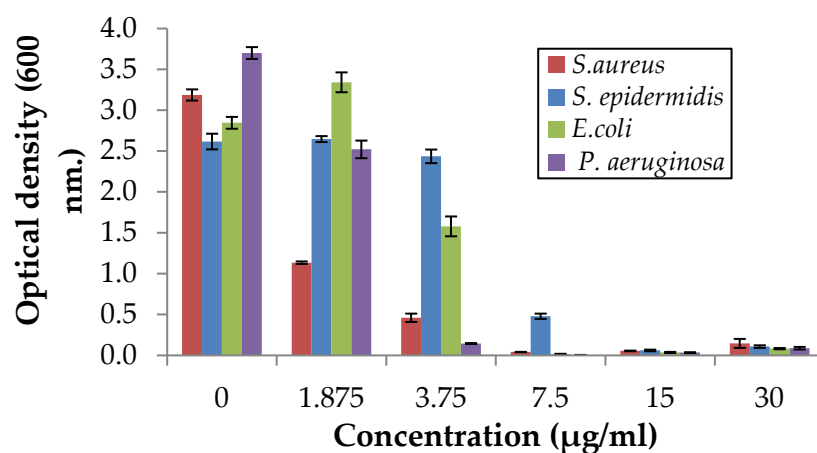


Figure 10. Optical density after 24 h with varying concentrations of AgNPs against *S. aureus*, *S. epidermidis*, *E. coli*, and *P. aeruginosa*.

4. Conclusions

In summary, the present study demonstrates the green synthesis of the AgNPs using aqueous Ceylon olive fruit extract. The novel synthesis is a simple, cost-effective, and environmentally friendly alternative to the conventional chemical approach. AgNPs were thoroughly characterized using UV–visible absorption, XRD, EDX, SEM, and FTIR. XRD studies revealed that AgNPs have a crystalline face-centered cubic structure, and the average crystallite size was 19 nm. SEM analysis showed that the particles were in the nanorange and diverse in shape. The study indicated that the morphology of AgNPs critically depended on pH, temperature, and the volume of extract used for the synthesis. FTIR spectra attested to the occurrence of functional groups in the plant extracts and demonstrated that proteins, flavonoids, and phenols were mainly responsible for the reduction and stabilization. AgNPs synthesized using Ceylon olive extract further exhibited a significantly higher antibacterial effect against Gram-negative bacterial strains compared to Gram-positive bacterial strains. The broth dilution method determined that Gram-negative bacterial strains had a lower minimum inhibitory concentration (MIC) than Gram-positive bacteria, correlating with the observed zone of inhibition. A larger zone of inhibition corresponded to a smaller MIC value, and vice versa.

These biofunctionalized AgNPs show promise for the treatment of microbial-mediated infections. In future research, we plan to conduct additional experiments to optimize the antibacterial activity of AgNPs considering their growth conditions. Furthermore, we may explore the incorporation of synthesized AgNPs into rubber latex for the production of bactericidal gloves.

Author Contributions: Conceptualization, Research design: C.A.N.F. and K.M.F. Investigation, Methodology and analysis: C.Y. and K.M.F. Experimental data collection: K.M.F. and G.W. Writing—original draft: K.M.F. Review and editing: K.M.F., C.A.G., C.Y., U.K.S., G.K.P., I.S., N.G., S.M.R. and O.F. All authors have read and agreed to the published version of the manuscript.

Funding: This research received no external funding.

Data Availability Statement: Data are contained within the article.

Acknowledgments: The authors are grateful to the Coconut Research Institute for the financial support for research and to the Wayamba University of Sri Lanka for providing the facility for sample analysis.

Conflicts of Interest: The authors declare no conflicts of interest.

References

1. Linklater, D.P.; Baulin, V.A.; Le Guével, X.; Fleury, J.B.; Hanssen, E.; Nguyen, T.H.P.; Juodkakis, S.; Bryant, G.; Crawford, R.J.; Stoodley, P.; et al. Antibacterial Action of Nanoparticles by Lethal Stretching of Bacterial Cell Membranes. *Adv. Mater.* **2020**, *32*, 2005679. [[CrossRef](#)] [[PubMed](#)]
2. Naganthran, A.; Verasoundarapandian, G.; Khalid, F.E.; Masarudin, M.J.; Zulkharnain, A.; Nawawi, N.M.; Karim, M.; Abdullah, C.A.C.; Ahmad, S.A. Synthesis, Characterization and Biomedical Application of Silver Nanoparticles. *Materials* **2022**, *15*, 427. [[CrossRef](#)] [[PubMed](#)]
3. Baranwal, A.; Srivastava, A.; Kumar, P.; Bajpai, V.K. Prospects of Nanostructure Materials and Their Composites as Antimicrobial Agents. *Front. Microbiol.* **2018**, *9*, 422. [[CrossRef](#)] [[PubMed](#)]
4. Mba, I.E.; Nweze, E.I. Nanoparticles as Therapeutic Options for Treating Multidrug-Resistant Bacteria: Research Progress, Challenges, and Prospects. *World J. Microbiol. Biotechnol.* **2021**, *37*, 1–30. [[CrossRef](#)] [[PubMed](#)]
5. El-kader, F.H.A.; Hakeem, N.A.; Elashmawi, I.S.; Menazea, A.A. Spectrochimica Acta Part A: Molecular and Biomolecular Spectroscopy Synthesis and Characterization of PVK / AgNPs Nanocomposites Prepared by Laser Ablation. *Spectrochim. ACTA PART A Mol. Biomol. Spectrosc.* **2016**, *138*, 331–339. [[CrossRef](#)] [[PubMed](#)]
6. Yadav, T.P.; Yadav, R.M.; Singh, D.P. Mechanical Milling: A Top Down Approach for the Synthesis of Nanomaterials and Nanocomposites. *Nanosci. Nanotechnol.* **2012**, *2*, 22–48. [[CrossRef](#)]
7. Benetti, G.; Cavaliere, E.; Banfi, F.; Gavioli, L. Antimicrobial Nanostructured Coatings: A Gas Phase Deposition and Magnetron Sputtering Perspective. *Materials* **2020**, *13*, 784. [[CrossRef](#)]
8. Torrisi, G.; Cavaliere, E.; Banfi, F.; Benetti, G.; Raciti, R.; Gavioli, L.; Terrasi, A. Ag Cluster Beam Deposition for TCO/Ag/TCO Multilayer. *Sol. Energy Mater. Sol. Cells* **2019**, *199*, 114–121. [[CrossRef](#)]
9. Valerini, D.; Tamarro, L.; Vigliotta, G.; Picariello, E.; Banfi, F.; Cavaliere, E.; Ciambriello, L.; Gavioli, L. Ag Functionalization of Al-Doped ZnO Nanostructured Coatings on PLA Substrate for Antibacterial Applications. *Coatings* **2020**, *10*, 1238. [[CrossRef](#)]

10. Ghosh, S.; Ahmad, R.; Zeyauallah, M.; Khare, S.K. Microbial Nano-Factories: Synthesis and Biomedical Applications. *Front. Chem.* **2021**, *9*, 626834. [[CrossRef](#)]
11. Ramanathan, S.; Gopinath, S.C.B. Potentials in Synthesizing Nanostructured Silver Particles. *Microsyst. Technol.* **2017**, *23*, 4345–4357. [[CrossRef](#)]
12. Anbu, P.; Gopinath, S.C.B.; Salimi, M.N.; Letchumanan, I.; Subramaniam, S. Green Synthesized Strontium Oxide Nanoparticles by *Elodea Canadensis* Extract and Their Antibacterial Activity. *J. Nanostructure Chem.* **2022**, *12*, 365–373. [[CrossRef](#)]
13. Shah, M.; Fawcett, D.; Sharma, S.; Tripathy, S.K. Green Synthesis of Metallic Nanoparticles via Biological Entities. *Materials* **2015**, *8*, 7278–7308. [[CrossRef](#)]
14. Hamedi, S.; Shojaosadati, S.A. Rapid and Green Synthesis of Silver Nanoparticles Using *Diospyros Lotus* Extract: Evaluation of Their Biological and Catalytic Activities. *Polyhedron* **2019**, *171*, 172. [[CrossRef](#)]
15. Huq, M.A.; Ashrafudoulla, M.; Rahman, M.M.; Balusamy, S.R.; Akter, S. Green Synthesis and Potential Antibacterial Applications of Bioactive Silver Nanoparticles: A Review. *Polymers* **2022**, *14*, 742. [[CrossRef](#)] [[PubMed](#)]
16. Miu, B.A.; Dinischiotu, A. New Green Approaches in Nanoparticles Synthesis: An Overview. *Molecules* **2022**, *27*, 6472. [[CrossRef](#)] [[PubMed](#)]
17. Abeska, Y.Y.; Cavas, L. Artificial Neural Network Modelling of Green Synthesis of Silver Nanoparticles by Honey. *Neural Netw. World* **2022**, *32*, 1–14. [[CrossRef](#)]
18. Devi, M.; Devi, S.; Sharma, V.; Rana, N.; Bhatia, R.K.; Bhatt, A.K. Green Synthesis of Silver Nanoparticles Using Methanolic Fruit Extract of *Aegle Marmelos* and Their Antimicrobial Potential against Human Bacterial Pathogens. *J. Tradit. Complement. Med.* **2020**, *10*, 158–165. [[CrossRef](#)]
19. Saidu, F.K.; Mathew, A.; Parveen, A.; Valiyathra, V.; Thomas, G.V. Novel Green Synthesis of Silver Nanoparticles Using Clammy Cherry (*Cordia Oblivata* Willd) Fruit Extract and Investigation on Its Catalytic and Antimicrobial Properties. *SN Appl. Sci.* **2019**, *1*, 1368. [[CrossRef](#)]
20. Dutta, T.; Chowdhury, S.K.; Ghosh, N.N.; Chattopadhyay, A.P.; Das, M.; Mandal, V. Green Synthesis of Antimicrobial Silver Nanoparticles Using Fruit Extract of *Glycosmis Pentaphylla* and Its Theoretical Explanations. *J. Mol. Struct.* **2022**, *1247*, 131361. [[CrossRef](#)]
21. Masum, M.I.; Siddiqua, M.M.; Ali, K.A.; Zhang, Y.; Abdallah, Y.; Ibrahim, E.; Qiu, W.; Yan, C.; Li, B. Biogenic Synthesis of Silver Nanoparticles Using *Phyllanthus Emblica* Fruit Extract and Its Inhibitory Action against the Pathogen *Acidovorax Oryzae* Strain RS-2 of Rice Bacterial Brown Stripe. *Front. Microbiol.* **2019**, *10*, 1–18. [[CrossRef](#)]
22. Bharadwaj, K.K.; Rabha, B.; Pati, S.; Choudhury, B.K.; Sarkar, T.; Gogoi, S.K.; Kakati, N.; Baishya, D.; Kari, Z.A.; Edinur, H.A. Green Synthesis of Silver Nanoparticles Using *Diospyros Malabarica* Fruit Extract and Assessments of Their Antimicrobial, Anticancer and Catalytic Reduction of 4-Nitrophenol (4-Np). *Nanomaterials* **2021**, *11*, 1999. [[CrossRef](#)] [[PubMed](#)]
23. Rajakannu, S.; Shankar, S.; Perumal, S.; Subramanian, S.; Dhakshinamoorthy, G.P. Biosynthesis of Silver Nanoparticles Using *Garcinia Mangostana* Fruit Extract and Their Antibacterial, Antioxidant Activity. *Int. J. Curr. Microbiol. Appl. Sci.* **2015**, *4*, 944–952.
24. Dayanand, M. Fruit Extract: Potential Role in Catalytic Degradation of Methylene. *IJPSR* **2022**, *13*, 3187–3193.
25. Chouhan, S.; Guleria, S. Green Synthesis of AgNPs Using *Cannabis Sativa* Leaf Extract: Characterization, Antibacterial, Anti-Yeast and α -Amylase Inhibitory Activity. *Mater. Sci. Energy Technol.* **2020**, *3*, 536–544. [[CrossRef](#)]
26. Hemlata; Meena, P.R.; Singh, A.P.; Tejavath, K.K. Biosynthesis of Silver Nanoparticles Using *Cucumis Prophetarum* Aqueous Leaf Extract and Their Antibacterial and Antiproliferative Activity against Cancer Cell Lines. *ACS Omega* **2020**, *5*, 5520–5528. [[CrossRef](#)]
27. Yassin, M.T.; Al-Otibi, F.O.; Mostafa, A.A.F.; Al-Askar, A.A. Facile Green Synthesis of Silver Nanoparticles Using Aqueous Leaf Extract of *Origanum Majorana* with Potential Bioactivity against Multidrug Resistant Bacterial Strains. *Crystals* **2022**, *12*, 603. [[CrossRef](#)]
28. Naveed, M.; Bukhari, B.; Aziz, T.; Zaib, S.; Mansoor, M.A.; Khan, A.A.; Shahzad, M.; Dablood, A.S.; Alruways, M.W.; Almalki, A.A.; et al. Green Synthesis of Silver Nanoparticles Using the Plant Extract of *Acer Oblongifolium* and Study of Its Antibacterial and Antiproliferative Activity via Mathematical Approaches. *Molecules* **2022**, *27*, 4226. [[CrossRef](#)]
29. Melkamu, W.W.; Bitew, L.T. Green Synthesis of Silver Nanoparticles Using *Hagenia Abyssinica* (Bruce) J.F. Gmel Plant Leaf Extract and Their Antibacterial and Anti-Oxidant Activities. *Heliyon* **2021**, *7*, e08459. [[CrossRef](#)]
30. Ahmad, M.A.; Salmiati, S.; Marpongahtun, M.; Salim, M.R.; Lolo, J.A.; Syafiuddin, A. Green Synthesis of Silver Nanoparticles Using *Muntingia Calabura* Leaf Extract and Evaluation of Antibacterial Activities. *Biointerface Res. Appl. Chem.* **2020**, *10*, 6253–6261.
31. De Fernando, F.L.; Caroline, A.B.; Claudia, A.L.C.; Marta, C.T.D.; Eliana, J.S.-A. Evaluation of Nutritional Composition, Bioactive Compounds and Antimicrobial Activity of *Elaeocarpus Serratus* Fruit Extract. *Afr. J. Food Sci.* **2019**, *13*, 30–37. [[CrossRef](#)]
32. Biswas, S.K.; Chowdhury, A.; Das, J.; Chowdhury, A.; Raihan, S.Z.; Muhit, M.A. Phytochemical Investigation with Assessment of Cytotoxicity and Antibacterial Activities of the Ethanol Extract of *Elaeocarpus Serratus*. *Am. J. Plant Physiol.* **2012**, *7*, 47–52. [[CrossRef](#)]
33. Jayashree, I.; Nadu, T. Jayashree et al. Evaluation of Antimicrobial Potential of *Elaeocarpus Serratus* L. *IJPSR* **2014**, *5*, 3467–3472.
34. Manoharan, A.L.; Thamburaj, S.; Muniyandi, K.; Jagadeesan, G.; Sathyanarayanan, S.; Nataraj, G.; Thangaraj, P. Antioxidant and Antimicrobial Investigations of *Elaeocarpus tectorius* (Lour.) Poir. Fruits against Urinary Tract Infection Pathogens. *Biocatal. Agric. Biotechnol.* **2019**, *20*, 101260. [[CrossRef](#)]
35. Geetha, D.H.; Rajeswari, M.; Jayashree, I. Chemical Profiling of *Elaeocarpus serratus* L. by GC-MS. *Asian Pac. J. Trop. Biomed.* **2013**, *3*, 985–987. [[CrossRef](#)] [[PubMed](#)]
36. Sircar, B.; Mandal, M.; Mondal, M.A.; Mandal, S. Biosynthesis of *Elaeocarpus floribundus* Mediated Silver Nanoparticles with Broad Antibacterial Spectrum. *Acta Sci. Pharm. Sci.* **2017**, *1*, 59–67.

37. Kumar, T.S.; Shanmugam, S.; Palvannan, T.; Kumar, V.M.B. Evaluation of Antioxidant Properties of *Elaeocarpus ganitrus* Roxb. Leaves. *Iran. J. Pharm. Res.* **2008**, *7*, 211–215.
38. Singh, B.; Chopra, A.; Ishar, M.P.S.; Sharma, A.; Raj, T. Pharmacognostic and Antifungal Investigations of *Elaeocarpus ganitrus* (Rudrakasha). *Indian J. Pharm. Sci.* **2010**, *72*, 261–265. [[CrossRef](#)] [[PubMed](#)]
39. Jayasinghe, L.; Amarasinghe, N.R.; Arundathie, B.G.S.; Rupasinghe, G.K.; Jayatilake, N.H.A.N.; Fujimoto, Y. Antioxidant Flavonol Glycosides from *Elaeocarpus serratus* and *Filicium decipiens*. *Nat. Prod. Res.* **2012**, *26*, 717–721. [[CrossRef](#)]
40. Doğan Çalhan, S.; Gündoğan, M. Biosynthesis of Silver Nanoparticles Using *Onosma sericeum* Willd. and Evaluation of Their Catalytic Properties and Antibacterial and Cytotoxic Activity. *Turk. J. Chem.* **2020**, *44*, 1587–1600. [[CrossRef](#)]
41. Bodke, M.; Gawai, U.; Patil, A.; Dole, B. Estimation of Accurate Size, Lattice Strain Using Williamson-Hall Models, SSP and TEM of Al Doped ZnO Nanocrystals. *Mater. Technol.* **2018**, *106*, 602. [[CrossRef](#)]
42. Rautela, A.; Rani, J.; Debnath (Das), M. Green Synthesis of Silver Nanoparticles from Tectona Grandis Seeds Extract: Characterization and Mechanism of Antimicrobial Action on Different Microorganisms. *J. Anal. Sci. Technol.* **2019**, *10*, 5. [[CrossRef](#)]
43. Salvesen, I.; Vadstein, O. Evaluation of Plate Count Methods for Determination of Maximum Specific Growth Rate in Mixed Microbial Communities, and Its Possible Application for Diversity Assessment. *J. Appl. Microbiol.* **2000**, *88*, 442–448. [[CrossRef](#)]
44. Arif, R.; Uddin, R. A Review on Recent Developments in the Biosynthesis of Silver Nanoparticles and Its Biomedical Applications. *Med. Devices Sens.* **2021**, *4*, e10158. [[CrossRef](#)]
45. Abaid, R.; Malik, M.; Iqbal, M.A.; Malik, M.; Shahwani, Z.; Ali, T.Z.; Morsy, K.; Capangpangan, R.Y.; Alguno, A.C.; Choi, J.R. Biosynthesizing Cassia Fistula Extract-Mediated Silver Nanoparticles for MCF-7 Cell Lines Anti-Cancer Assay. *ACS Omega* **2023**, *8*, 17317–17326. [[CrossRef](#)]
46. Malik, M.; Iqbal, M.A.; Malik, M.; Raza, M.A.; Shahid, W.; Choi, J.R.; Pham, P.V. Biosynthesis and Characterizations of Silver Nanoparticles from *Ammonia squamosa* Leaf and Fruit Extracts for Size-Dependent Biomedical Applications. *Nanomaterials* **2022**, *12*, 616. [[CrossRef](#)]
47. Vijayakumar, S.; Chen, J.; González Sánchez, Z.I.; Tungare, K.; Bhor, M.; Durán-Lara, E.F.; Anbu, P. *Moringa oleifera* Gum Capped MgO Nanoparticles: Synthesis, Characterization, Cyto- and Ecotoxicity Assessment. *Int. J. Biol. Macromol.* **2023**, *233*, 123514. [[CrossRef](#)]
48. Femi-Adepoju, A.G.; Dada, A.O.; Otun, K.O.; Adepoju, A.O.; Fatoba, O.P. Green Synthesis of Silver Nanoparticles Using Terrestrial Fern (*Gleichenia pectinata* (Willd.) C. Presl.): Characterization and Antimicrobial Studies. *Heliyon* **2019**, *5*, e01543. [[CrossRef](#)]
49. Sarwer, Q.; Amjad, M.S.; Mehmood, A.; Binish, Z.; Mustafa, G.; Farooq, A.; Qaseem, M.F.; Abasi, F.; Pérez de la Lastra, J.M. Green Synthesis and Characterization of Silver Nanoparticles Using Myrsine Africana Leaf Extract for Their Antibacterial, Antioxidant and Phytotoxic Activities. *Molecules* **2022**, *27*, 7612. [[CrossRef](#)]
50. Ravichandran, V.; Vasanthi, S.; Shalini, S.; Shah, S.A.A.; Tripathy, M.; Paliwal, N. Green Synthesis, Characterization, Antibacterial, Antioxidant and Photocatalytic Activity of Parkia Speciosa Leaves Extract Mediated Silver Nanoparticles. *Results Phys.* **2019**, *15*, 102565. [[CrossRef](#)]
51. Mohammed, A.E.; Ameen, F.; Aabed, K.; Saad, R. In-Silico Predicting as a Tool to Develop Plant-Based Biomedicines and Nanoparticles: *Lycium shawii* Metabolites. *Biomed. Pharmacother.* **2022**, *150*, 113008. [[CrossRef](#)]
52. Mahiuddin, M.; Saha, P.; Ochiai, B. Green Synthesis and Catalytic Activity of Silver Nanoparticles Based on *Piper chaba* Stem Extracts. *Nanomaterials* **2020**, *10*, 1777. [[CrossRef](#)]
53. Balavijayalakshmi, J.; Ramalakshmi, V. Carica Papaya Peel Mediated Synthesis of Silver Nanoparticles and Its Antibacterial Activity against Human Pathogens. *J. Appl. Res. Technol.* **2017**, *15*, 413–422. [[CrossRef](#)]
54. Chinnasamy, G.; Chandrasekharan, S.; Bhatnagar, S. Biosynthesis of Silver Nanoparticles from Melia Azedarach: Enhancement of Antibacterial, Wound Healing, Antidiabetic and Antioxidant Activities. *Int. J. Nanomed.* **2019**, *14*, 9823–9836. [[CrossRef](#)]
55. Jin, Y.; Li, B.; Saravanakumar, K.; Hu, X.; Mariadoss, A.V.A.; Wang, M.H. Cytotoxic and Antibacterial Activities of Starch Encapsulated Photo-Catalyzed Phytogenic Silver Nanoparticles from *Paeonia lactiflora* Flowers. *J. Nanostructure Chem.* **2022**, *12*, 375–387. [[CrossRef](#)]
56. Anuradha, J.; Abbasi, T.; Abbasi, S.A. An Eco-Friendly Method of Synthesizing Gold Nanoparticles Using an Otherwise Worthless Weed Pistia (*Pistia stratiotes* L.). *J. Adv. Res.* **2015**, *6*, 711–720. [[CrossRef](#)]
57. Sharifi-Rad, M.; Pohl, P.; Epifano, F.; Álvarez-Suarez, J.M. Green Synthesis of Silver Nanoparticles Using *Astragalus tribuloides* Delile. Root Extract: Characterization, Antioxidant, Antibacterial, and Anti-Inflammatory Activities. *Nanomaterials* **2020**, *10*, 2383. [[CrossRef](#)]
58. Shehzad, A.; Qureshi, M.; Jabeen, S.; Ahmad, R.; Alabdallal, A.H.; Alfary, M.A.; Al-Suhaimi, E. Synthesis, Characterization and Antibacterial Activity of Silver Nanoparticles Using *Rhazya stricta*. *PeerJ* **2018**, *2018*, e6086. [[CrossRef](#)]
59. Prasad, K.S.; Pathak, D.; Patel, A.; Dalwadi, P.; Prasad, R.; Patel, P.; Selvaraj, K. Biogenic Synthesis of Silver Nanoparticles Using *Nicotiana tobaccum* Leaf Extract and Study of Their Antibacterial Effect. *Afr. J. Biotechnol.* **2011**, *10*, 8122–8130.
60. Singh, A.; Gaud, B.; Jaybhaye, S. Optimization of Synthesis Parameters of Silver Nanoparticles and Its Antimicrobial Activity. *Mater. Sci. Energy Technol.* **2020**, *3*, 232–236. [[CrossRef](#)]
61. Bawazeer, S.; Rauf, A.; Shah, S.U.A.; Shawky, A.M.; Al-Awthan, Y.S.; Bahattab, O.S.; Uddin, G.; Sabir, J.; El-Esawi, M.A. Green Synthesis of Silver Nanoparticles Using *Tropaeolum majus*: Phytochemical Screening and Antibacterial Studies. *Green Process. Synth.* **2021**, *10*, 85–94. [[CrossRef](#)]
62. Xu, L.; Wang, Y.Y.; Huang, J.; Chen, C.Y.; Wang, Z.X.; Xie, H. Silver Nanoparticles: Synthesis, Medical Applications and Biosafety. *Theranostics* **2020**, *10*, 8996–9031. [[CrossRef](#)]

63. Jasuja, N.D.; Gupta, D.K.; Reza, M.; Joshi, S.C. Green Synthesis of AgNPs Stabilized with Biowaste and Their Antimicrobial Activities. *Braz. J. Microbiol.* **2014**, *45*, 1325–1332. [[CrossRef](#)]
64. Ibrahim, H.M.M. Green Synthesis and Characterization of Silver Nanoparticles Using Banana Peel Extract and Their Antimicrobial Activity against Representative Microorganisms. *J. Radiat. Res. Appl. Sci.* **2015**, *8*, 265–275. [[CrossRef](#)]
65. Velu, M.; Lee, J.H.; Chang, W.S.; Lovanh, N.; Park, Y.J.; Jayanthi, P.; Palanivel, V.; Oh, B.T. Fabrication, Optimization, and Characterization of Noble Silver Nanoparticles from Sugarcane Leaf (*Saccharum officinarum*) Extract for Antifungal Application. *3 Biotech* **2017**, *7*, 1–9. [[CrossRef](#)]
66. Eya'ane Meva, F.; Segnou, M.L.; Ebongue, C.O.; Ntumba, A.A.; Kedi, P.B.E.; Deli, V.; Etoh, M.A.; Mpondo, E.M. Spectroscopic Synthetic Optimizations Monitoring of Silver Nanoparticles Formation from *Megaphrynium macrostachyum* Leaf Extract. *Rev. Bras. Farmacogn.* **2016**, *26*, 640–646. [[CrossRef](#)]
67. Marciniak, L.; Nowak, M.; Trojanowska, A.; Tylkowski, B.; Jastrzab, R. The Effect of Ph on the Size of Silver Nanoparticles Obtained in the Reduction Reaction with Citric and Malic Acids. *Materials* **2020**, *13*, 5444. [[CrossRef](#)]
68. Alqadi, M.K.; Abo Noqtah, O.A.; Alzoubi, F.Y.; Alzoubi, J.; Aljarrah, K. PH Effect on the Aggregation of Silver Nanoparticles Synthesized by Chemical Reduction. *Mater. Sci. Pol.* **2014**, *32*, 107–111. [[CrossRef](#)]
69. Khalil, M.M.H.; Ismail, E.H.; El-Baghdady, K.Z.; Mohamed, D. Green Synthesis of Silver Nanoparticles Using Olive Leaf Extract and Its Antibacterial Activity. *Arab. J. Chem.* **2014**, *7*, 1131–1139. [[CrossRef](#)]
70. Vanlalveni, C.; Lallianrawna, S.; Biswas, A.; Selvaraj, M.; Changmai, B.; Rokhum, S.L. Green Synthesis of Silver Nanoparticles Using Plant Extracts and Their Antimicrobial Activities: A Review of Recent Literature. *RSC Adv.* **2021**, *11*, 2804–2837. [[CrossRef](#)] [[PubMed](#)]
71. Pimprikar, P.S.; Joshi, S.S.; Kumar, A.R.; Zinjarde, S.S.; Kulkarni, S.K. Influence of Biomass and Gold Salt Concentration on Nanoparticle Synthesis by the Tropical Marine Yeast *Yarrowia lipolytica* NCIM 3589. *Colloids Surfaces B Biointerfaces* **2009**, *74*, 309–316. [[CrossRef](#)]
72. Mothana, R.A.; Hussain, H. Phyto-Extract-Mediated Synthesis of Silver Nanoparticles Using Aqueous Extract of *Sanvitalia procumbens*, and Characterization, Optimization and Photocatalytic Degradation of Azo Dyes Orange G and Direct Blue-15. *Molecules* **2021**, *26*, 6144.
73. Davidović, S.; Lazić, V.; Vukoje, I.; Papan, J.; Anhrenkiel, S.P.; Dimitrijević, S.; Nedeljković, J.M. Dextran Coated Silver Nanoparticles—Chemical Sensor for Selective Cysteine Detection. *Colloids Surf. B Biointerfaces* **2017**, *160*, 184–191. [[CrossRef](#)]
74. More, P.R.; Pandit, S.; De Filippis, A.; Franci, G.; Mijakovic, I.; Galdiero, M. Silver Nanoparticles: Bactericidal and Mechanistic Approach against Drug Resistant Pathogens. *Microorganisms* **2023**, *11*, 369. [[CrossRef](#)]
75. Mandal, D.; Kumar Dash, S.; Das, B.; Chattopadhyay, S.; Ghosh, T.; Das, D.; Roy, S. Bio-Fabricated Silver Nanoparticles Preferentially Targets Gram Positive Depending on Cell Surface Charge. *Biomed. Pharmacother.* **2016**, *83*, 548–558. [[CrossRef](#)]
76. Vega-Baudrit, J.; Gamboa, S.M.; Rojas, E.R.; Martinez, V.V. Synthesis and Characterization of Silver Nanoparticles and Their Application as an Antibacterial Agent. *Int. J. Biosens. Bioelectron.* **2019**, *5*, 166–173. [[CrossRef](#)]
77. Yarrappagaari, S.; Gutha, R.; Narayanaswamy, L.; Thopireddy, L.; Benne, L.; Mohiyuddin, S.S.; Vijayakumar, V.; Saddala, R.R. Eco-Friendly Synthesis of Silver Nanoparticles from the Whole Plant of *Cleome viscosa* and Evaluation of Their Characterization, Antibacterial, Antioxidant and Antidiabetic Properties. *Saudi J. Biol. Sci.* **2020**, *27*, 3601–3614. [[CrossRef](#)]
78. Soliman, I.; Gunathilake, C.; Paudel, P.R. Nanoarchitectonics of planar organic electrochemical transistors for biological applications and electrochemical sensors. *J. Solid State Electrochem.* **2023**, *023*, 05771–9. [[CrossRef](#)]
79. Gopinath, V.; Priyadarshini, S.; Loke, M.F.; Arunkumar, J.; Marsili, E.; MubarakAli, D.; Velusamy, P.; Vadivelu, J. Biogenic Synthesis, Characterization of Antibacterial Silver Nanoparticles and Its Cell Cytotoxicity. *Arab. J. Chem.* **2017**, *10*, 1107–1117. [[CrossRef](#)]

Disclaimer/Publisher's Note: The statements, opinions and data contained in all publications are solely those of the individual author(s) and contributor(s) and not of MDPI and/or the editor(s). MDPI and/or the editor(s) disclaim responsibility for any injury to people or property resulting from any ideas, methods, instructions or products referred to in the content.